J. Fluid Mech. (1974), *vol.* 66, *part* 4, *pp.* 707–724
Printed in Great Britain

A numerical model of instability in axisymmetric jets

By A. J. GRANT

Shell Research Ltd, Thornton Research Centre, P.O. Box 1, Chester CH1 3SH

(Received 21 July 1973 and in revised form 4 June 1974)

The detailed flow fields associated with instability in axisymmetric jets are realized by numerical integration of the time-dependent Navier–Stokes equations.

The mechanism of amplification of small disturbances is shown to be two-dimensional for a thin boundary layer profile and conclusions regarding three-dimensionality which have been inferred from recent models of axisymmetrical systems are clarified.

The computed flow field is shown to be dominated by the large-scale vortex ring structure which has been observed experimentally. Although the wavelength of vortex shedding is found to be slightly variable owing to the randomness of the initial perturbation, the results are shown to agree closely with experiment.

1. Introduction

The experimental study of instability and transition to turbulence in circular jets and the observation of persistent orderly structure in the turbulent regime have resulted in an extensive literature by many authors. However, theoretical studies have, as always, been limited by the intractability of the Navier–Stokes equations and only two approximate time-dependent solutions have been obtained. The first is that of classical linearized theory to which the major contribution is found in the paper by Batchelor & Gill (1962) and the second involves the inviscid representation of the flow by discrete arrays of point vortices and is typified by the work of Beavers & Wilson (1970). In the present paper the effects of both nonlinearity and viscosity are investigated by numerical integration of the complete time-dependent equations.

The model is limited to axisymmetrical flow since, with the present generation of high-speed computers, the analysis of three-dimensional unsteady flows requires prohibitive amounts of computer storage and time. This limitation immediately raises the question of whether the model can provide physically realistic solutions. The answer has been given, in part, by Batchelor & Gill since their analysis predicts that a 'top-hat' jet profile will amplify axisymmetric disturbances but that, for profiles varying slowly in a radial direction, only non-axisymmetric types of instability are possible. These results have been confirmed experimentally by Crow & Champagne (1971).

The geometrical restriction also removes any possibility of studying the effects

of vortex stretching. However, Browand (1966) found, in his study of a separated shear layer, that many of the nonlinear features observed could, in fact, be explained in terms of purely two-dimensional mechanisms. This is also true of the results obtained by Crow & Champagne which indicate large-scale orderly structure evolving through several modes over a very wide range of Reynolds number. Thus following the terminology of Coles (1965) the free shear layer transition may be described as a 'spectral evolution' rather than the 'catastrophic transition' which typifies wall flows. Therefore, it appears that, although vortex stretching is neglected in the present case, many of the experimentally observed features may still be modelled by the axisymmetrical geometry.

The numerical integration is carried out by the method of finite differences and thus the results are inherently limited in temporal and spatial resolution. This is particularly obvious for the spatial case since the typical dimensions of fine-scale turbulence are orders of magnitude smaller than the smallest grid spacings that can be considered. However, again considering the experimental results it is clear that, for the particular geometry chosen, the high wavenumber cut-off should not seriously affect the validity of the results.

2. Basic equations

The basic equations are the Navier–Stokes equations expressed in terms of the Stokes stream function, ψ, and of the vorticity, ω. The vorticity transport equation in cylindrical co-ordinates is

$$\frac{\partial \omega}{\partial t}+\frac{\partial}{\partial z}(u\omega)+\frac{\partial}{\partial r}(v\omega)=\frac{1}{\mathrm{Re}}\left(\nabla^2\omega-\frac{\omega}{r^2}\right), \tag{1}$$

where

$$\nabla^2=\frac{\partial^2}{\partial r^2}+\frac{1}{r}\frac{\partial}{\partial r}+\frac{\partial^2}{\partial z^2}, \tag{2}$$

u and v denote the velocity components in the axial and radial directions, z and r, respectively. The Reynolds number, Re, is based on the nozzle diameter D, the kinematic viscosity ν, and the potential nozzle velocity U_0. All quantities are dimensionless with reference to D and U_0. The velocities are related to the stream function by

$$u=\frac{1}{r}\frac{\partial \psi}{\partial r}, \quad v=-\frac{1}{r}\frac{\partial \psi}{\partial z}. \tag{3}$$

The stream function therefore satisfies the following equation:

$$\omega=\frac{1}{r}\left(\frac{\partial^2\psi}{\partial z^2}+\frac{\partial^2\psi}{\partial r^2}-\frac{1}{r}\frac{\partial \psi}{\partial r}\right). \tag{4}$$

3. The finite difference equations

The basic set of equations to be solved comprises equations (1), (3) and (4). The finite difference form of this set varies to a certain extent spatially owing to boundary conditions (see § 4) but in general the method is based upon the work of Fromm (1969*b*) and is as follows.

Specification of the mesh of points at which variables may be defined is given schematically in figure 1. Hence, the difference approximation of equation (4) is

$$\omega_{i,j,k} = \frac{1}{r_j}\left\{\frac{\psi_{i,j+1,k}-2\psi_{i,j,k}+\psi_{i,j-1,k}}{(fa)^2}+\frac{\psi_{i+1,j,k}-2\psi_{i,j,k}+\psi_{i-1,j,k}}{a^2} - \frac{\psi_{i,j-1,k}-\psi_{i,j+1,k}}{2r_j fa}\right\}. \quad (5)$$

The index k specifies the time step number, and a and fa the spatial increments in the axial and radial directions respectively. In equation (1) the diffusion part is represented in an analogous manner to (5), i.e.

$$\frac{1}{Re}\left(\nabla^2\omega-\frac{\omega}{r^2}\right) = \frac{1}{Re}\left\{\frac{\omega_{i,j+1,k}-2\omega_{i,j,k}+\omega_{i,j-1,k}}{(fa)^2}+\frac{\omega_{i,j-1,k}-\omega_{i,j+1,k}}{2r_j fa} + \frac{\omega_{i+1,j,k}-2\omega_{i,j,k}+\omega_{i-1,j,k}}{a^2}-\frac{\omega_{i,j,k}}{r_j^2}\right\}. \quad (6)$$

The approximation of the convective terms is identical to that of Fromm (1969*b*) (i.e. of fourth-order, explicit form) and therefore the left-hand side of equation (1) gives

$$\frac{\omega_{i,j,k+1}-\omega_{i,j,k}}{\Delta t}+\frac{1}{a}(F_{i+\frac{1}{2},j,k}-F_{i-\frac{1}{2},j,k})+\frac{1}{fa}(F_{i,j-\frac{1}{2},k}-F_{i,j+\frac{1}{2},k}), \quad (7)$$

where F denotes the following general notation:

$$F_{i-\frac{1}{2},j,k} = \frac{a}{\Delta t}[A\omega_{i-2,j,k}+B\omega_{i-1,j,k}+C\omega_{i,j,k}]$$

with

$$A = \tfrac{1}{12}(-\alpha-\tfrac{1}{2}\alpha^2+\alpha^3+\tfrac{1}{2}\alpha^4),$$
$$B = (\tfrac{1}{2}\alpha+\tfrac{2}{3}\alpha^2-\tfrac{1}{6}\alpha^4),$$
$$C = \tfrac{1}{12}(7\alpha-\tfrac{15}{2}\alpha^2-\alpha^3+\tfrac{3}{2}\alpha^4),$$

and

$$\alpha = \alpha_{i-\frac{1}{2},j,k} = \left(\frac{\Delta t}{a}\right)u_{i-\frac{1}{2},j,k}. \quad (8)$$

The values of $u_{i\pm\frac{1}{2},j,k}$ and $v_{i,j\pm\frac{1}{2},k}$ as required in equation (7) may be obtained by averaging over the four nearest nodes and can subsequently be written in terms of the stream function by using equation (3), e.g.

$$u_{i-\frac{1}{2},j,k} = \frac{1}{4fa}\left\{\frac{1}{r_{j-\frac{1}{2}}}(\psi_{i-1,j-1,k}-\psi_{i-1,j,k}+\psi_{i,j-1,k}-\psi_{i,j,k}) + \frac{1}{r_{j+\frac{1}{2}}}(\psi_{i-1,j,k}-\psi_{i-1,j+1,k}+\psi_{i,j,k}-\psi_{i,j+1,k})\right\}.$$

4. Initial and boundary conditions

The specification of boundary conditions for the type of physical field discussed in this paper presents a great many difficulties. Ideally, one would like to obtain the solution to the problem of a jet discharging into an infinite medium. However, the method of approach requires that the problem be transformed into a pseudo boundary-value problem within the domain of the computational grid.

In order to obtain a determinate system some approximations have to be made along the edges of the grid.

(*a*) Dealing first with *ED* (see figure 1), the problem arises that $\partial^2\omega/\partial z^2$ and $\partial^2\psi/\partial z^2$ (which appear in equations (1) and (4) respectively) cannot be evaluated using space-centred differences (see equations (5) and (6)) since no mesh points exist beyond *ED*. However, it is known that these second derivatives are small everywhere and therefore one can make the empirical approximation that, along *ED*, they may be neglected in comparison with the other terms appearing on the right-hand sides of equations (1) and (4), i.e.

$$\frac{\partial^2\psi}{\partial z^2} \ll \frac{\partial^2\psi}{\partial r^2} - \frac{1}{r}\frac{\partial\psi}{\partial r}, \tag{9}$$

$$\frac{\partial^2\omega}{\partial z^2} \ll \frac{\partial^2\omega}{\partial r^2} + \frac{1}{r}\frac{\partial\omega}{\partial r} - \frac{\omega}{r^2}. \tag{10}$$

From a computational point of view this is equivalent to setting both $\partial^2\omega/\partial z^2$ and $\partial^2\psi/\partial z^2$ equal to zero on *ED*. This approximation should not be interpreted as a rigorous boundary condition imposed on the problem (which would exclude certain solutions) but rather as an approximation to the values of the appropriate terms in the equations of motion. The vorticity equation is still solved numerically along *ED* although the convective terms are now approximated by simple one-sided differences as follows:

$$\frac{\omega_{i,j,k+1}-\omega_{i,j\,k}}{\Delta t} + \frac{u_{i,j,k}}{a}(\omega_{i,j,k}-\omega_{i-1,j,k}) + \frac{v_{i-\frac{1}{2},j,k}}{2fa}(\omega_{i,j-1,k}-\omega_{i,j+1,k}). \tag{11}$$

(*b*) Along *CD* a similar problem arises and in this near irrotational region the following empirical values are used in solving the equations of motion:

$$\frac{\partial^2\omega}{\partial r^2} = 0 \quad \text{and} \quad \frac{\partial^2\psi}{\partial r^2} = 0. \tag{12}$$

Again one-sided differencing is applied to the vorticity equation.

(*c*) Along *BC*, i.e. the horizontal wall adjacent to the jet, equation (4) yields the no-slip equation:

$$\omega_{BC} = \frac{1}{r}\frac{\partial^2\psi}{\partial z^2}. \tag{13}$$

Several different formulations of this equation have been used in the present model including the Taylor series expansion employed previously by Gerrard (1971) and Macagno & Hung (1967). However the simpler formula derived from Lagrange's interpolation formula (see Roache 1972) has proved equally

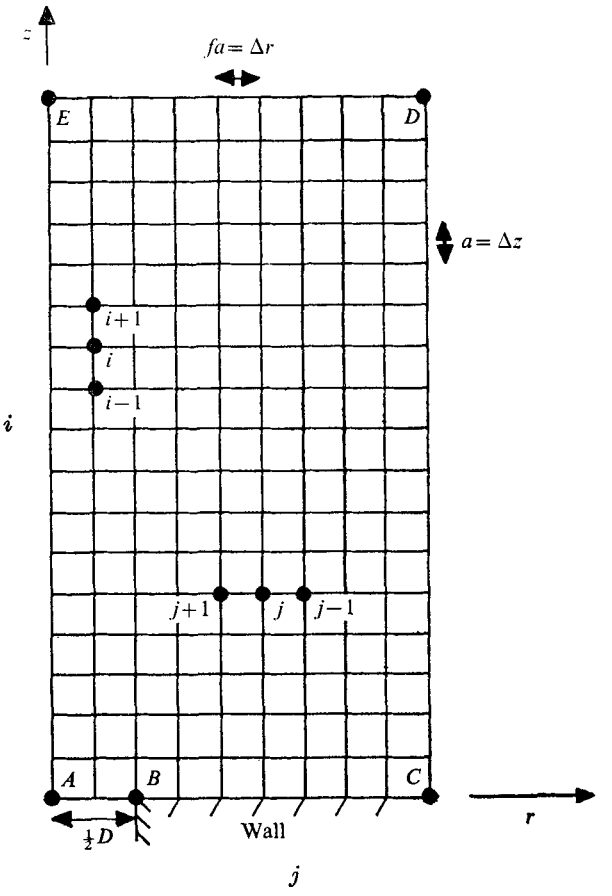

FIGURE 1. Computational grid for jet half-space.

successful for this very slow-flow region. Representing the wall surface by the subscript I, one obtains

$$\omega_{I,j,k} = \frac{1}{a^2 r_j}(-\tfrac{7}{2}\psi_{I,j,k} + 4\psi_{I+1,j,k} - \tfrac{1}{2}\psi_{I+2,j,k}). \tag{14}$$

(*d*) Along AB, i.e. the jet orifice, the initial profiles of the dependent variables are stated in the form $\omega = \omega(r)$ and $\psi = \psi(r)$ only. At point B the vorticity is fixed to be zero, i.e. separation of the flow is forced at the corner.

(*e*) Second-order terms. At the mesh points next to the wall and outflow regions there are insufficient adjacent points to use fourth-order approximations and thus the procedure used by Fromm (1969*b*) has been adopted whereby five-point second-order approximations are applied, i.e. the two-dimensional form of Leith's method (Roache 1972).

5. Iteration technique

At each step in time the vorticity function is advanced directly on integration of equation (1) and by using these new results the stream function is then evaluated by successive point over-relaxation (Fox 1962).

An error estimate, Q, is first obtained from equation (5), i.e.

$$Q_{i,j} = \omega_{i,j,k+1} - \frac{1}{r_j}\left\{\frac{\psi_{i,j+1,k} - 2\psi_{i,j,k} + \psi_{i,j-1,k}}{(fa)^2}\right.$$

$$\left. + \frac{\psi_{i+1,j,k} - 2\psi_{i,j,k} + \psi_{i-1,j,k}}{a^2} - \frac{\psi_{i,j-1,k} - \psi_{i,j+1,k}}{2r_j fa}\right\}. \quad (15)$$

The new stream function is hence

$$\psi_{i,j}^{n+1} = \psi_{i,j}^{n} - \tfrac{1}{2}\gamma a^2 r_j Q_{i,j}^{n}\left\{\frac{f^2}{1+f^2}\right\}, \quad (16)$$

where γ is the over-relaxation factor and n is the iteration index. The iteration procedure follows a row-by-row sweep of the computational grid and is terminated when the modifications to ψ fall below a certain predetermined threshold. A value of 1·52 for γ has been used throughout.

6. Streaklines

The motion of a particle is governed by the differential equations

$$\frac{dz}{dt} = u(z(t), r(t), t), \quad (17)$$

$$\frac{dr}{dt} = v(z(t), r(t), t), \quad (18)$$

where u and v are given by equation (3). $z(t)$ and $r(t)$ denote the position of the particle at time t. In order to compute a streakline, appropriate initial conditions are defined, viz.

$$z(t_0) = z_0 \quad \text{and} \quad r(t_0) = r_0 \quad (19)$$

and particles are introduced at this point at predetermined intervals of time. The particle paths are then calculated at each time step by simple forward differencing of equations (17) and (18) using linear interpolation over four adjacent points for the velocity contributions.

7. Numerical accuracy and stability

The basic difference scheme has been chosen so as to minimize phase error effects as much as possible since these are the primary cause of computational noise. Obviously this is of prime importance where large-scale periodic behaviour is expected to dominate.

The computational stability of the linearized finite difference equations can be analysed using the stability analysis of von Neumann, i.e. vorticity transport is assumed to take place with u and v locally constant. Unfortunately the complexity of the fourth-order schemes makes the algebraic solution of the amplification matrix completely intractable and thus a numerical evaluation of the stability bounds of the matrix is necessary. These have been well documented

by Fromm (1969*a*) for the equations in the absence of molecular diffusion. The diffusional terms by themselves result in the familiar limit (see Gerrard 1971)

$$\Delta t < Ka^2Re, \tag{20}$$

where K is approximately constant. Equation (20) implies that the maximum rate of diffusion is limited to an advance of one mesh length per time step.

In the present model, however, the maximum permissible time step is governed not by the fourth-order differences but by the behaviour of the second-order difference equations required near the boundaries of the grid (§4(*e*)). The difference scheme is the two-dimensional form of Leith's method, which is known to be unconditionally unstable in the absence of viscous forces unless a time-splitting approach is adopted. However, by inclusion of the viscous terms this inherent instability can be damped without recourse to the time-splitting form. By retaining only the contributions of the second derivatives in equation (6), and by expanding for small wavenumbers, wave analysis then gives the following analytical limit:

$$\alpha\beta < \frac{\Delta t}{Re}\left(\frac{1}{(fa)^2}+\frac{1}{a^2}\right), \tag{21}$$

where β is the radial equivalent of equation (8). This equation has been found to agree extremely closely with upper bounds obtained directly from computations with the full nonlinear equations.

Finally, in §5 it was stated that the iterative sequence is terminated when successive modifications to ψ fall below a certain predetermined threshold. This value is expressed by the maximum allowable error bound on $|Q^n_{i,j}|$ and the present results have been obtained using $|Q^n_{i,j}| \leqslant 0{\cdot}03$.

8. Results and discussion

Several initial velocity profiles have been modelled with markedly differing results and these can be explained in terms of the specific profiles shown in figure 2. It may be seen that, since the vorticity is constrained to be zero at the corner (§4(*d*)), the depicted velocity profiles show no discontinuity at this point. However, in terms of finite differences this degree of precision could only be achieved with an unacceptably fine mesh size and therefore a lower accuracy must be tolerated in this localized region than in the rest of the computational grid.

The results discussed below have all been obtained using radial increments of $\frac{1}{12}$. Two values for the axial increments have been used, namely, $a = \frac{1}{12}$ and $a = \frac{1}{6}$. The computational half-space comprised 21 radial increments and either 81 axial increments (for $a = \frac{1}{12}$) or 41 axial increments (for $a = \frac{1}{6}$).

The steady-state (laminar) solution at a Reynolds number of 600 for profile I is plotted in terms of the stream function in figure 3 (all figures will refer to $a = \frac{1}{12}$ unless otherwise stated). The equivalent result for profile II is shown in figure 4† and the corresponding isodines, or contours or constant vorticity, are

† The numbers on the computer-drawn curves in this and other figures are not intended to be legible, but it may help the reader to know that the increments in the dependent variable between neighbouring curves are all equal.

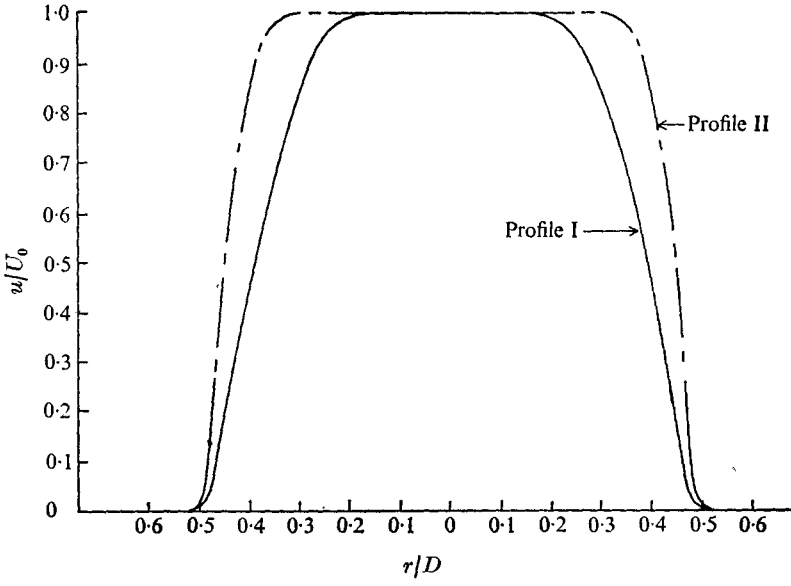

FIGURE 2. Initial velocity profiles.

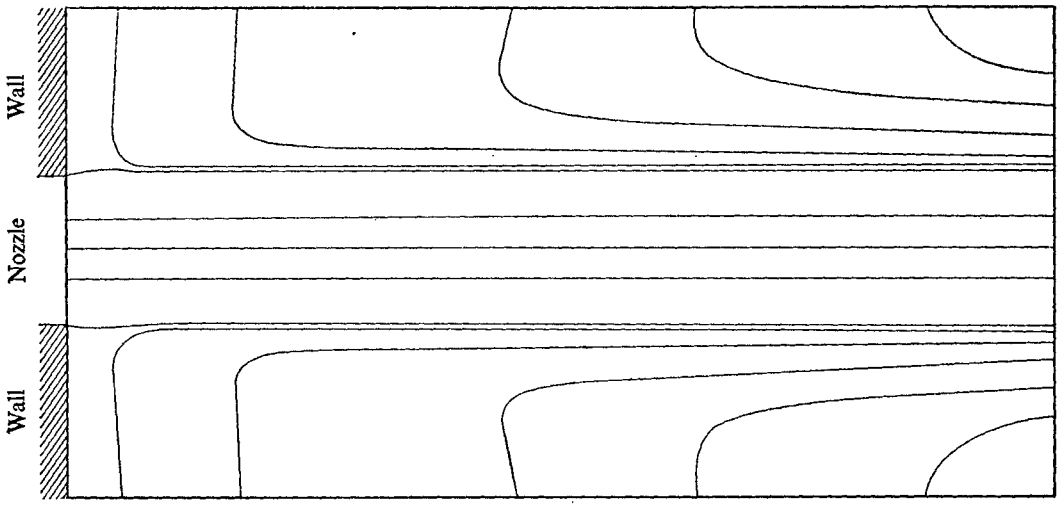

FIGURE 3. Stream function, Reynolds number = 600, laminar flow (velocity profile I).

shown in figure 5. The Reynolds number of 400 which is represented in figure 5 is the critical value of that number for profile II since any increase immediately results in prolonged unstable flow. Of course, the field of view is limited to the domain of integration and thus the concept of a critical value must be accepted with this limitation. In figures 6(*a*) and (*b*) the subsequent effects of a step function increase in Reynolds number from 400 to 450 at zero time are plotted. The contour denoted by a value of $-1{\cdot}70$ demonstrates the delineation of fluid dynamic instability by an initial stretching out (figure 6(*a*)) of the isodine until eventually it sheds the detached vortex shown in figure 6(*b*).

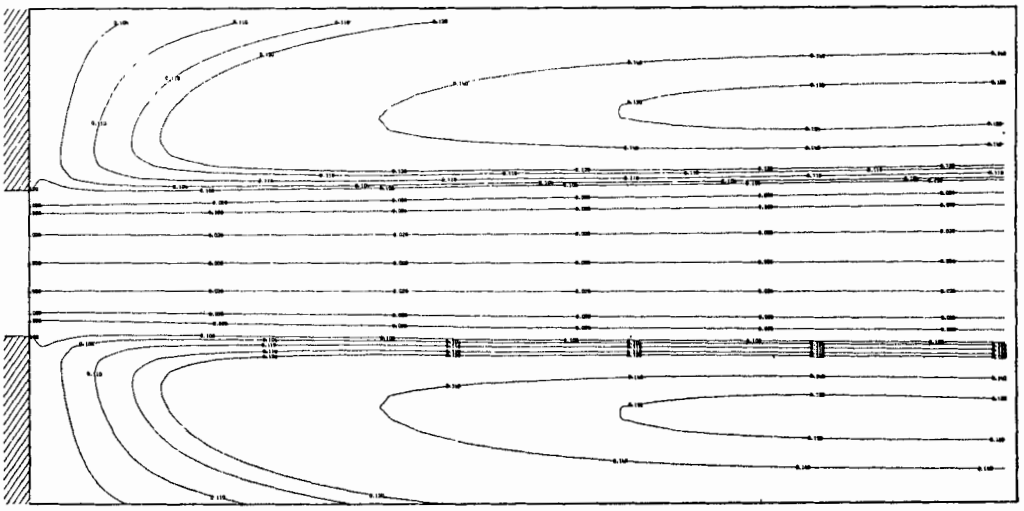

FIGURE 4. Stream function, Reynolds number = 400, laminar flow (velocity profile II).

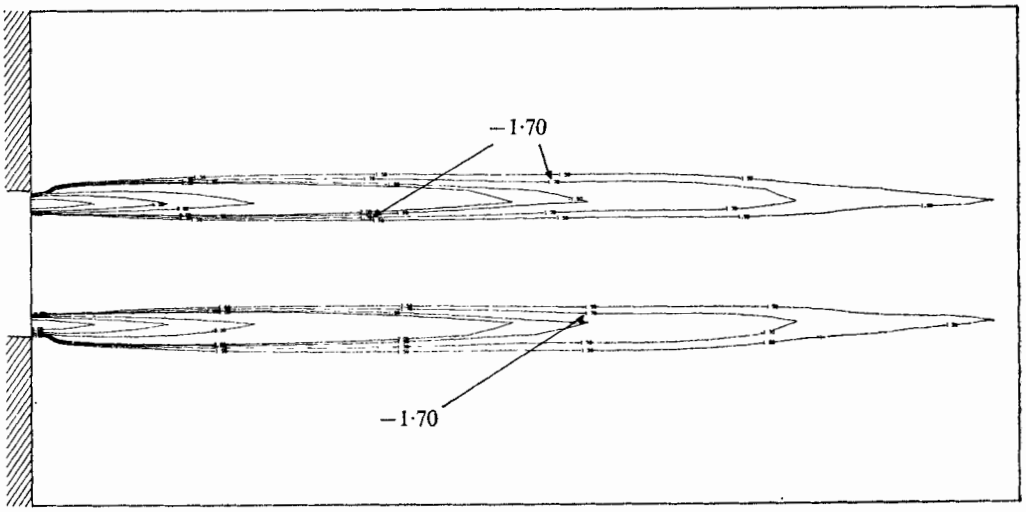

FIGURE 5. Isodines, Reynolds number = 400, laminar flow (velocity profile II).

Figures 7 (*a*)–(*g*) show the vorticity history (again for profile II) at a Reynolds number of 1400 and the fundamental mechanism of instability is again clearly apparent. It is also clear from these results and the corresponding streamlines of figure 8 that a large-scale quasi-periodic structure is predominant.

In figure 9 an instantaneous vorticity distribution for profile II at a Reynolds number of 1400 but computed with $a = \frac{1}{6}$ is plotted. The same overall quasi-periodic structure is again apparent although the vorticity distribution is much 'noisier' than in figure 7. Although the average wavelength of the periodicity is the same as that of the more accurate grid the introduction of much larger errors can be established from the behaviour of the vortex centres as they are

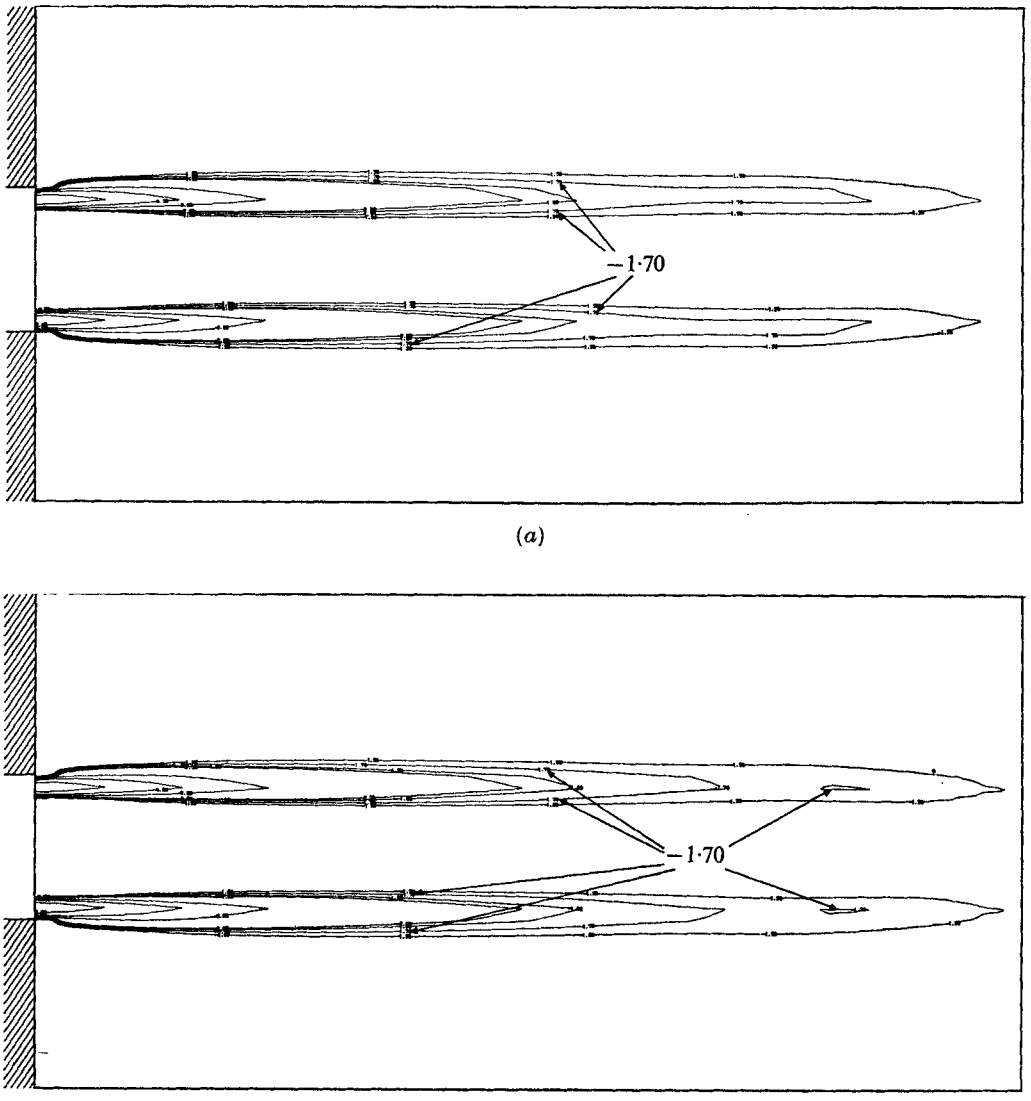

FIGURE 6. Isodines, Reynolds number = 450 (velocity profile II). (*a*) Time = 1·0; (*b*) time = 1·5.

convected downstream. For the finer mesh the centres show a slow decay as one would expect whereas several of those in figure 9 undergo an increase in vorticity which is, of course, excluded physically owing to the two-dimensional geometry. Nevertheless the onset of instability and the basic large-scale behaviour is consistent for the two mesh sizes.

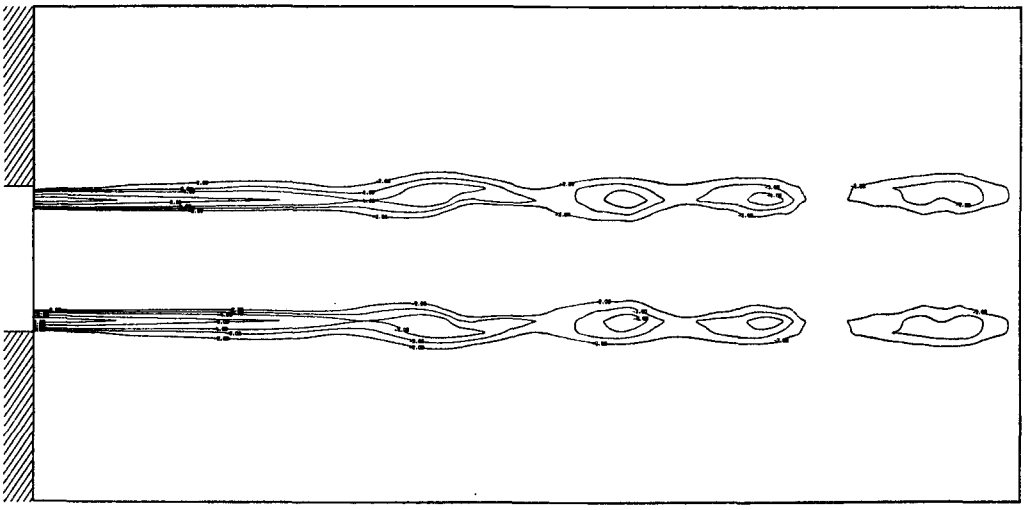

(*a*)

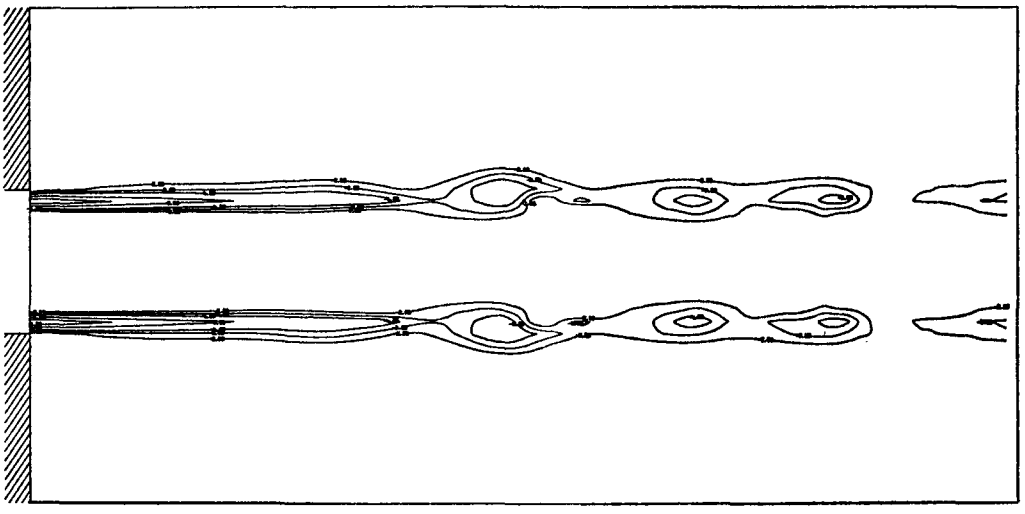

(*b*)

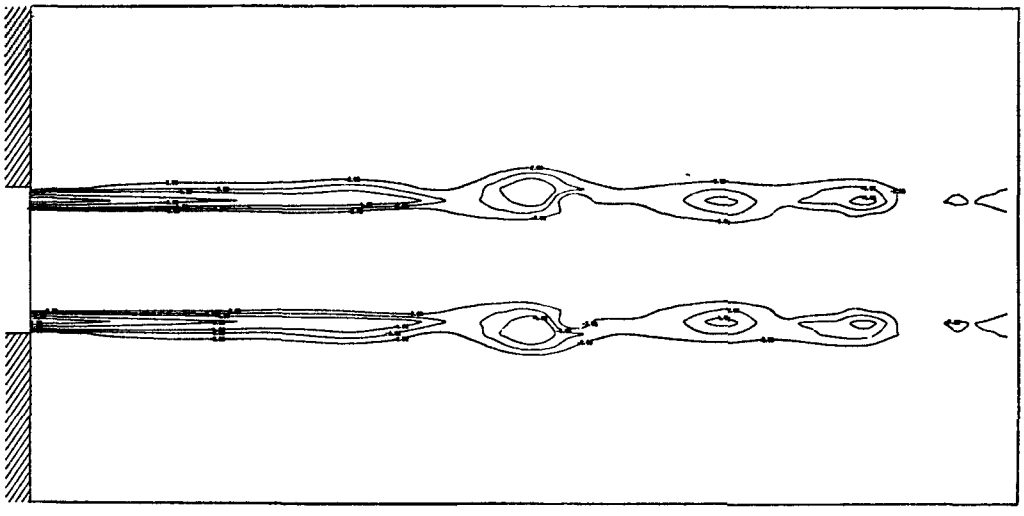

(*c*)

FIGURES 7(*a*)–(*c*). For legend see p. 719.

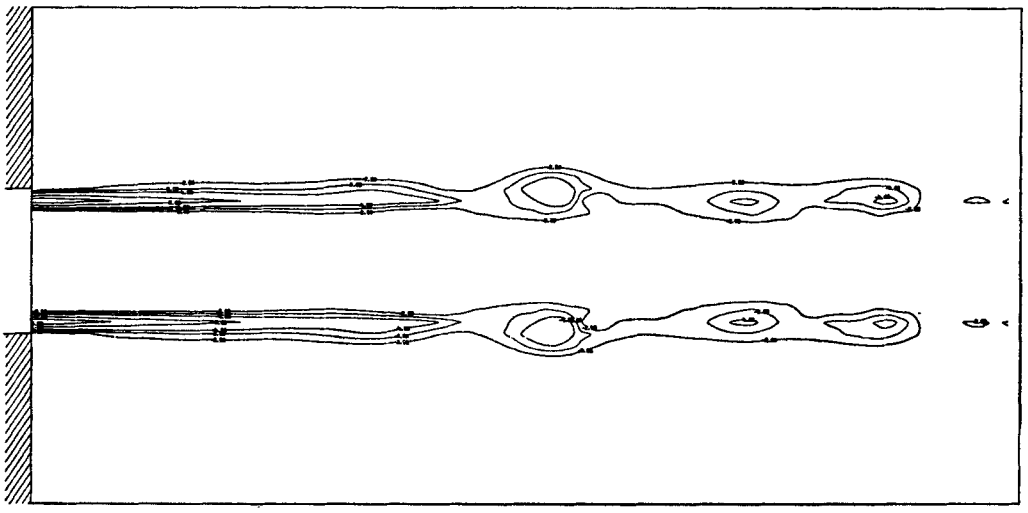

(*d*)

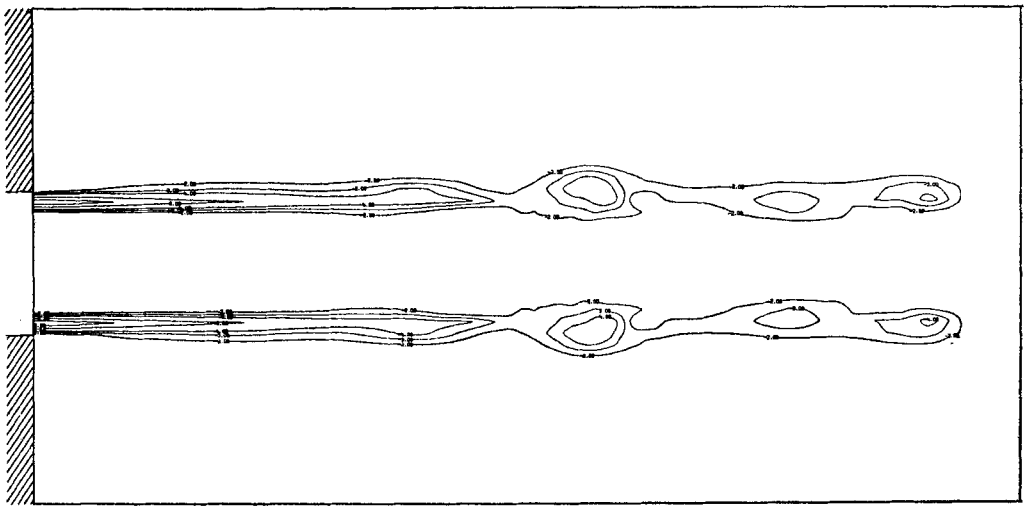

(*e*)

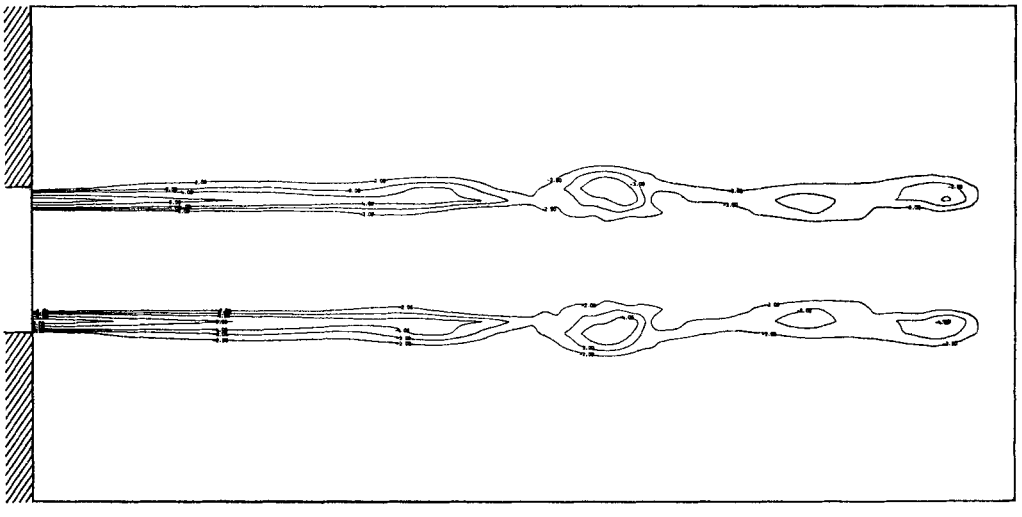

(*f*)

FIGURES 7(*d*)–(*f*). For legend see next page.

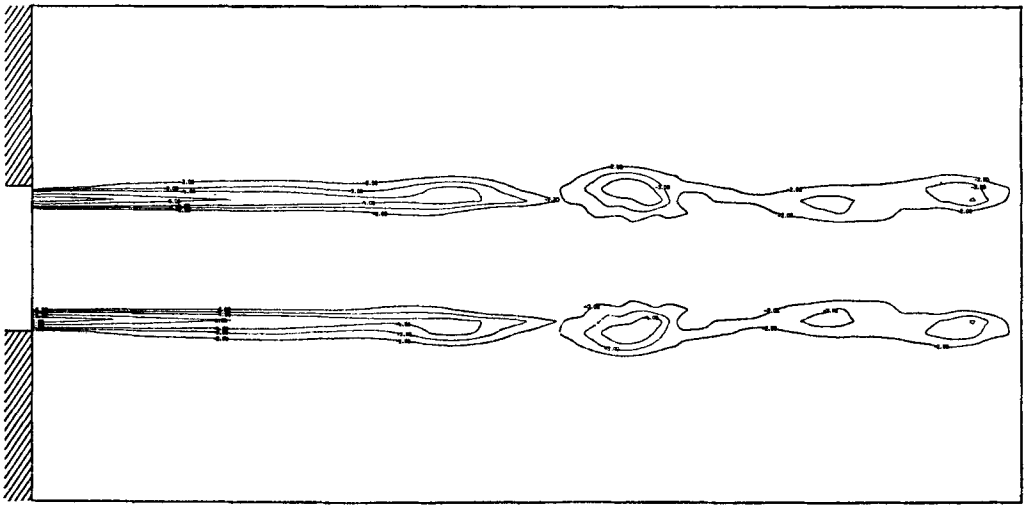

(*g*)

FIGURE 7. Isodines, Reynolds number = 1400 (velocity profile II). (*a*) Time = 0·6; (*b*) time = 1·0; (*c*) time = 1·2; (*d*) time = 1·5; (*e*) time = 1·8; (*f*) time = 2·1; (*g*) time = 2·4.

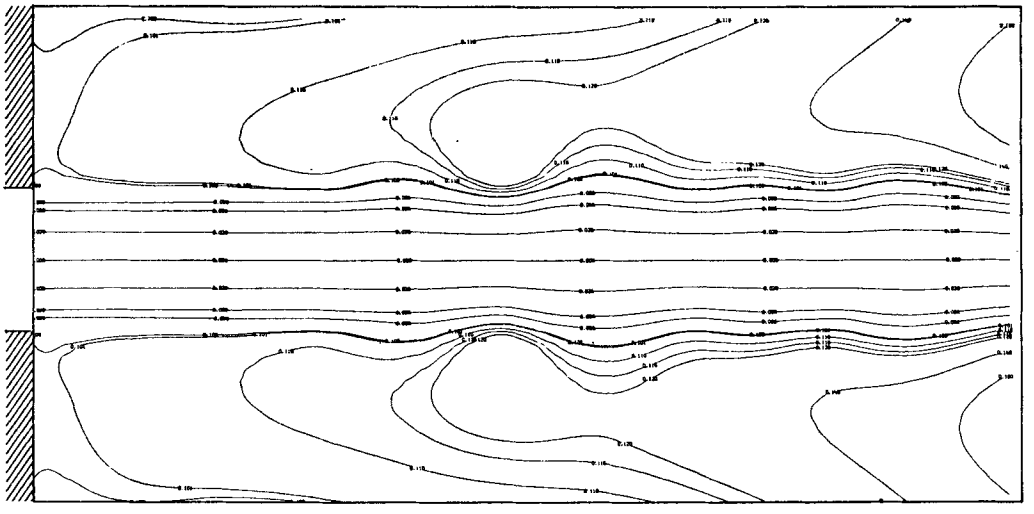

FIGURE 8. Stream function, Reynolds number = 1400, time = 1·0 (velocity profile II).

The amplification of small disturbances

Initially it was expected that, at some critical Reynolds number, any 'small disturbances' in the system (e.g. numerical round-off errors) would be amplified and hence an unsteady state would be established, and it is clear from the discussion above that, for profile II, this has indeed occurred. However, profile I exhibited no such instability and, instead, all solutions tended asymptotically towards a steady state, at least for the Reynolds numbers investigated, which were limited to a maximum value of 2500.

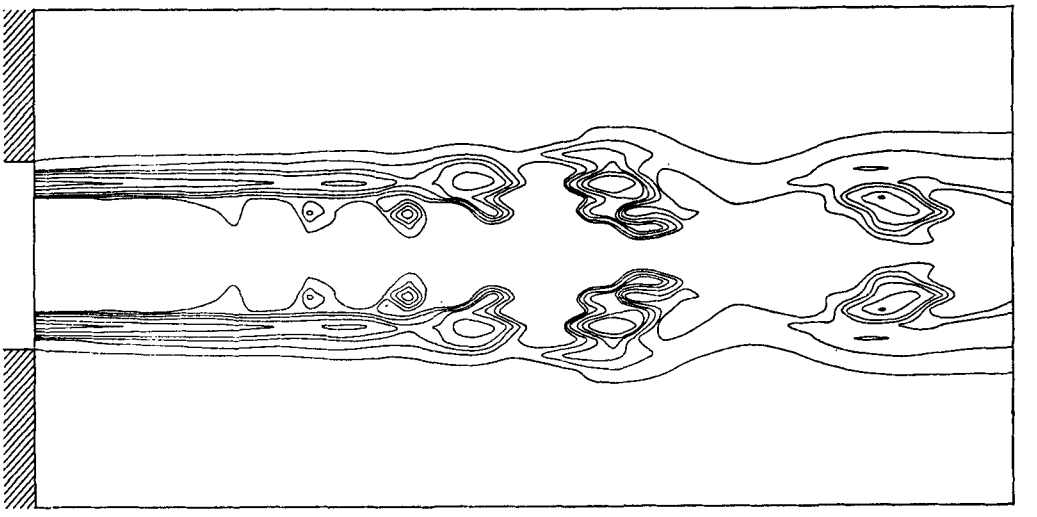

FIGURE 9. Isodines, Reynolds number = 1400, time = 0·8 (velocity profile II).

This failure to exhibit instability has also been found in two other numerical solutions of axisymmetrical flows. In the first example Rimon obtained solutions for the flow past both a sphere (Rimon & Cheng 1969) and a thin oblate spheroid (Rimon 1969); more recently Gerrard (1971) has investigated the motion from rest of a piston in a cylindrical tube. Rimon found it possible to simulate the initial stationary vortex system which is characteristic of blunt-body flows but failed entirely to model any shedding of vorticity. Gerrard encountered the same difficulty in his configuration but found further that the introduction of 'artificial' disturbances into his system in the form of deliberately added random noise immediately caused shedding to take place. Following this example, random noise was also added to the present model with profile I and again vortex shedding became apparent. It should be noted that the resultant deviations from a laminar structure were several orders of magnitude greater than the disturbance level.

It has been suggested by Gerrard that this behaviour can be attributed to the fact that "amplification is a three-dimensional effect which is excluded by the present (axisymmetric) computing method and has to be introduced artificially as random disturbances". Rimon, on the other hand, concluded that "the shedding of vorticity is a three-dimensional effect caused by three-dimensional disturbances". It is certainly now clear that vortex shedding can be two-dimensional and one may also conclude that the amplification mechanism can, as postulated by Batchelor & Gill, be two-dimensional given a 'thin' boundary layer profile.

The experiments of Crow & Champagne on water jets issuing from a glass tube showed that, with increasing Reynolds number, the evolution of an axisymmetric column of ring vortices may first occur through a helical mode. This three-dimensional amplification, which is excluded numerically and which corresponds to a thick boundary layer, shows that the conclusions reached by Gerrard and Rimon may well be correct for certain geometries but are not valid in any

generalized sense. It may be noted that the experiments of Becker & Massaro (1968) using a high contraction-ratio nozzle only demonstrated axisymmetrical instability.

Comparison with experiment

As mentioned earlier, the structure shown in figure 7 is not exactly periodic, i.e. successive wavelengths vary to a certain extent. This verifies the belief expressed in the previous section that the structure is triggered by numerical 'noise'. It also demonstrates the experimental advantages of acoustic forcing, i.e. phase locking, in order to obtain stroboscopic visualization. The strength of the individual vortices may also be seen to vary.

The dimensionless wavenumber, $\pi D/\lambda$, for the natural growth exhibited in figures 7 and 8 varies between 2·1 and 2·8 and this range agrees well with the value of 2·6 which has been found by Grant, Jones & Rosenfeld (1973), in jets with Reynolds numbers less than 2×10^4. Crow & Champagne state a value of 1·3 for Reynolds numbers in the range 10^4–10^5. This low value may well be due to an induction effect (see Becker & Massaro) whereby two vortices coalesce, thus causing an effective doubling of the wavelength. This has not been observed in the computed results but is probably excluded owing to the low Reynolds numbers that can be investigated, although it may also be a function of the disturbance level present in the experimental set-up. Figure 7 also implies a Strouhal number of about 0·55, which again agrees closely with the experimental value of 0·52 found by Grant *et al.* A flow at a Reynolds number of 1400 has also been observed experimentally by Beavers & Wilson, who obtained a Strouhal number of 0·63 using a sharp-edged circular orifice. These results may again be contrasted with the preferred value of 0·30 found by Crow & Champagne.

Secondary instabilities are recognizable in figures 7 (*b*), (*c*) and (*d*) where smaller vortex 'islands' are apparent in the intervals between the main vortices. These result from the way in which the isodines are drawn out to form elliptical islands with pronounced 'tails' which then detach to form secondary regions. At the flow rates shown these weak regions are quickly dissipated by molecular diffusion but one may conjecture that at higher rates they play a major part in producing inductive effects. An analogous effect has been computed by Fromm (1967) in a planar shear layer.

Any direct comparison with experimentally evaluated critical Reynolds numbers must be viewed carefully in the light of the findings discussed above. One must have equivalence of both initial boundary-layer thickness, i.e. vorticity distribution, and also disturbance amplitude and dimensionality before any conclusions can be drawn. For example, Viilu (1962) quotes a critical Reynolds number of about 11 but he almost certainly had Poiseuille flow at the nozzle exit and consequently a spiral instability. However, the present value does agree extremely well with the results of Beavers & Wilson for a very thin boundary layer. They found that, for Reynolds numbers between approximately 400 and 500, small irregularities became apparent in the flow and these occasionally broke up to form a small part of a column of vortex rings. They found further that these bursts occurred at random intervals over a very small range of

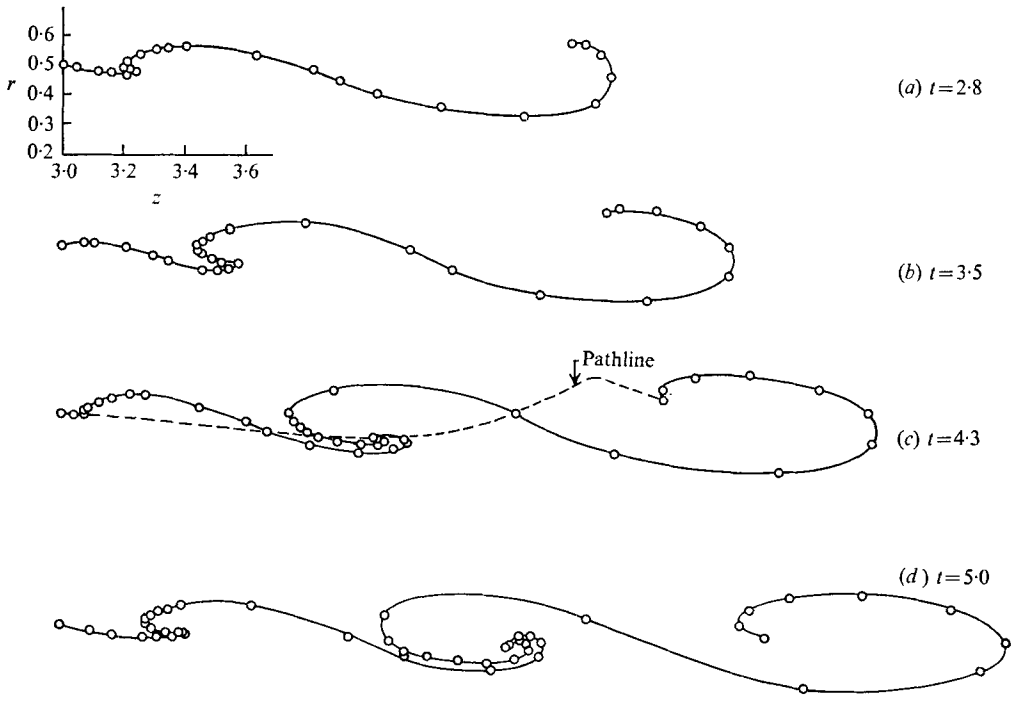

FIGURE 10. Streakline growth from $(r, z) = (\frac{1}{2}, 3)$, Reynolds number = 1850.

Reynolds numbers and that any subsequent increase in Reynolds number produced an uninterrupted train of vortex rings. Since Becker & Massaro found a critical value of about 600, one can, at least, say that the present predictions are within an experimentally acceptable range.

From an experimental viewpoint a system of axisymmetrical vortex rings is usually visualized by the introduction of smoke or dye into the flow. The calculation of such dyelines or streaklines has been discussed in §6 and is straightforward. However, the procedure demands extremely large amounts of computer time and storage if a large region of the flow field is to be mapped. Therefore, at present, the results have been limited to a small part of the free shear layer.

Figure 10 shows the evolution of a streakline for a series of particles released at $(r, z) = (\frac{1}{2}, 3)$ and the familiar rolling-up process which is typical of the point vortex model of Beavers & Wilson is displayed. In figure 10(*c*) the pathline of the initial particle is also traced and its simple trajectory underlines the comments of Hama (1962) on the intricacies of interpreting results which are due to purely relative motions. Indeed, Hama has shown that the rolling-up of a streakline is a necessary but not a sufficient condition for the existence of vorticity concentrations and of the formation of discrete vortices. Figure 11 shows a comparison between streakline behaviour and vorticity distribution at an instant in time and it can be seen that for this particular flow the streakline 'spirals' and vorticity maxima are coincident.

Finally, in assessing any results from a model of the type discussed in this paper one must take into account the somewhat heuristic specification of boundary

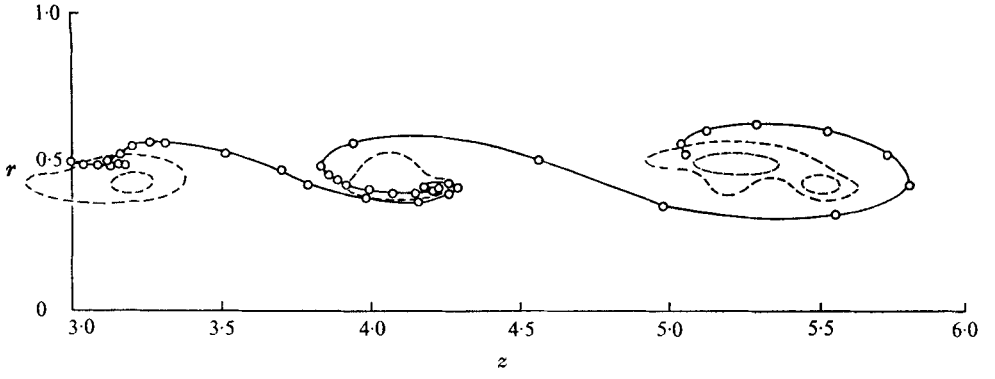

FIGURE 11. Streakline and vorticity relationship, Reynolds number 1850, time = 4·5.

conditions. This is important not only from the standpoint of the creation of numerical instabilities at the boundaries but also in the generation of parasitic eigenfunctions due to the transformation of a semi-infinite problem into a limited domain boundary-value problem. In the present model the problem of instability of the boundaries has not, in fact, arisen although it is particularly clear in figures 4 and 8 that in the vicinity of the separation streamline at the jet exit there is a local distortion of the flow due purely to numerical inaccuracy. However the eigenfunction nature of the problem is a much more significant effect.

Figure 3 shows the laminar flow streamlines corresponding to velocity profile I and it may be seen that the fluid entrained across the boundary, *CD*, is flowing reasonably parallel to the wall, *BC*, as one might intuitively expect. The streamlines are in fact showing a slight tendency to form a very large recirculation region, which is not altogether surprising since they must, by definition, be closed, i.e. they cannot terminate at a point in the flow. In figures 4 and 8, which show streamline behaviour for profile II, the recirculation region has become much smaller and one must question whether the calculated streamlines in the outer region are now representative of the real flow field. The approximation applied along *CD* (i.e. equation (12)) was reformulated to assume that the axial velocity changed little in a mesh width but this produced a symmetry condition along the boundary, thus reducing the recirculation region even more. However, the computed vorticity in this outer region was found to be, in all cases, negligible in comparison with that of the shear layer, and hence one may conclude that any eigenfunction effect on the actual jet transition is negligible although the far-field streamline behaviour is extremely dependent on the chosen boundary conditions.

This conclusion is borne out by the experimental studies of Iribarne *et al.* (1972) on the behaviour of an axisymmetrical pipe jet. Their results show the same basic large-scale vortex structure in the initial region of the jet as is found in the present study. Only at the region of re-attachment to the outer pipe wall does the basic structure break down and this may be attributed to the action of the wall vorticity.

I am greatly indebted to Dr J. L. J. Rosenfeld and Dr J. M. Jones for their invaluable assistance in the preparation of this paper. I should also like to thank Mr I. H. McBride for his help in the numerical computation.

REFERENCES

BATCHELOR, G. K. & GILL, A. E. 1962 *J. Fluid Mech.* **14**, 529–551.

BEAVERS, G. S. & WILSON, T. A. 1970 *J. Fluid Mech.* **44**, 97–112.

BECKER, H. A. & MASSARO, T. A. 1968 *J. Fluid Mech.* **31**, 435–448.

BROWAND, F. K. 1966 *J. Fluid Mech.* **26**, 281–308.

COLES, D. 1965 *J. Fluid Mech.* **21**, 385–426.

CROW, S. C. & CHAMPAGNE, F. H. 1971 *J. Fluid Mech.* **48**, 547–592.

FOX, L. 1962 *Numerical Solutions of Ordinary and Partial Differential Equations*, chap. 23. Pergamon.

FROMM, J. E. 1967 *Fluid Dynamics Transactions*, **3**, 169–191.

FROMM, J. E. 1969*a* *Phys. Fluids* (suppl. II), **12**, 3–12.

FROMM, J. E. 1969*b* *Phys. Fluids* (suppl. II), **12**, 113–119.

GERRARD, J. H. 1971 *J. Fluid Mech.* **50**, 625–644.

GRANT, A. J., JONES, J. M. & ROSENFELD, J. L. J. 1973 *Combustion Institute European Symposium*, pp. 548–552. Academic.

HAMA, F. R. 1962 *Phys. Fluids* **5**, 644–650.

IRIBARNE, A., FRANTISAK, F., HUMMEL, R. L. & SMITH, J. W. 1972 *A.I.Ch.E. J.* **18**, 689–698.

MACAGNO, E. O. & HUNG, T-K. 1967 *J. Fluid Mech.* **28**, 43–64.

RIMON, Y. 1969 *Phys. Fluids* (suppl. II), **12**, 65–75.

RIMON, Y. & CHENG, S. I. 1969 *Phys. Fluids*, **12**, 949–959.

ROACHE, P. J. 1972 *Computational Fluid Dynamics*, p. 142. Hermosa, Albuquerque.

VIILU, A. 1962 *J. Appl. Mech.* **29**, 506.